

Accepted Manuscript

Anterior lens capsule strains during simulated accommodation in porcine eyes

Antonio Pellegrino, Harvey John Burd, Laura Pinilla Cortés, Justin Christopher D'Antin, Nik Petrinic, Rafael I. Barraquer, Ralph Michael



PII: S0014-4835(17)30604-8

DOI: [10.1016/j.exer.2017.12.008](https://doi.org/10.1016/j.exer.2017.12.008)

Reference: YEXER 7248

To appear in: *Experimental Eye Research*

Received Date: 23 August 2017

Revised Date: 2 December 2017

Accepted Date: 22 December 2017

Please cite this article as: Pellegrino, A., Burd, H.J., Cortés, L.P., D'Antin, J.C., Petrinic, N., Barraquer, R.I., Michael, R., Anterior lens capsule strains during simulated accommodation in porcine eyes, *Experimental Eye Research* (2018), doi: 10.1016/j.exer.2017.12.008.

This is a PDF file of an unedited manuscript that has been accepted for publication. As a service to our customers we are providing this early version of the manuscript. The manuscript will undergo copyediting, typesetting, and review of the resulting proof before it is published in its final form. Please note that during the production process errors may be discovered which could affect the content, and all legal disclaimers that apply to the journal pertain.

Anterior lens capsule strains during simulated accommodation in porcine eyes

Antonio Pellegrino^{1*}, Harvey John Burd¹, Laura Pinilla Cortés², Justin Christopher D'Antin², Nik Petrinic¹, Rafael I. Barraquer^{2,3}, Ralph Michael²

¹Department of Engineering Science, University of Oxford, Oxford OX1 3PJ, United Kingdom

²Institut Universitari Barraquer, Universitat Autònoma de Barcelona, Barcelona, Spain

³Centro de Oftalmología Barraquer, Universitat Internacional de Catalunya, Barcelona, Spain

*antonio.pellegrino@eng.ox.ac.uk

Highlights

- A digital image correlation protocol has been developed to measure the spatial variation of mechanical strains induced in the anterior lens capsule during ex vivo radial stretching tests.
- Tests conducted on six porcine lenses are described. The observed strain fields in the anterior capsule indicate a consistent pattern of axial symmetry. The strain magnitudes increase with distance from the lens pole.
- Strain data obtained using this experimental technique could be used to check the veracity of computational models of accommodation.

Abstract

Experimental protocols have been developed to measure the spatial variation of the mechanical strains induced in the lens capsule during ex vivo lens stretching. The paper describes the application of these protocols to porcine lenses. The deformations and mechanical strains developed in the anterior capsule during each experiment were determined using full field digital image correlation techniques, by means of a speckle pattern applied to the lens surface. Several speckling techniques and illumination methods were assessed before a suitable combination was found. Additional data on the cross section shape of the anterior lens surface were obtained by Scheimpflug photography, to provide a means of correcting for lens curvature effects in the determination of the strains developed in the plane of the capsule. The capsule strains in porcine lenses exhibit non-linear behaviour, and hysteresis during loading and unloading. Peripheral regions experience higher magnitude strains than regions near the lens pole. The paper demonstrates the successful application of a procedure to make direct measurements of capsule strains simultaneously with ex vivo radial lens stretching. This experimental technique is applicable to future investigations on the mechanical characteristics of human lenses.

Keywords: lens capsule, accommodation, strain, porcine lens

1. Introduction

Accommodation of the human eye is achieved by a mechanism in which contraction of the ciliary muscle causes the radial forces applied to the lens, via the zonules, to relax. As a consequence, the lens assumes a thicker, more rounded shape with an increased optical power. The effectiveness of the accommodation process declines with age, however, with the consequence that, from late middle age onwards, the ability of the eye to accommodate becomes minimal.

The accommodation process relies on various mechanical interactions between the ciliary body, zonules, lens substance and lens capsule. An improved understanding of the detailed mechanism of accommodation, including the various mechanical interactions that occur and the way in which they develop with age, is needed to underpin the continued scientific study of the accommodation mechanism and to support the development of new forms of surgery (e.g. accommodating intraocular lenses) to improve, or even restore, the ability of the eye to accommodate in late middle age and elderly patients.

Experimental studies on the mechanical processes that occur during accommodation have been previously conducted using various forms of ex vivo lens stretching test (e.g. Manns et al. 2007; Ziebarth et al. 2008; Reilly et al., 2009; Augusteyn et al. 2011; Michael et al. 2012). Data from these studies provide information on the overall kinematic behaviour (i.e. relating to the deformations) of the lens, zonules and ciliary body during simulated accommodation. Measurements of the radial forces actually applied to the lens can also be made, although careful experimental design is needed to enable meaningful results to be obtained (Panilla Cortés et al. 2015). The current paper describes a further development of the ex vivo lens stretching protocol to include direct measurements on the displacement and strain fields induced in the lens capsule during simulated accommodation. The data obtained using this technique provide considerably more detail on the kinematic behaviour of the lens capsule than is obtained in conventional forms of the lens stretching test.

The current paper describes a preliminary program of tests conducted on porcine lenses. The principal purpose of the work is to establish and optimise the experimental protocols and data interpretation procedures prior to engaging in a test program on ex vivo human lenses. Data provided in the current paper are limited to tests on six porcine lenses; experiments on human lenses will form the basis of future work. Porcine and human lenses have certain similarities in anatomy and size (e.g. Sanchez et al. 2011). Human and porcine lens capsules have a similar

molecular composition (Hahn et al. 2015); they are both composed of a network of fibrous proteins, entactin/ nidogen and some heparin sulfate proteoglycans (Sueiras et al. 2015). Young porcine lenses exhibit a similar shear modulus gradient to the presbyopic human lens (Moffat, Atchison, and Pope 2002; Heys, Cram, and Truscott 2004; Pierscionek, Belaidi, and Bruun 2005; Weeber and van der Heijde 2007; Reilly and Ravi 2009). The Young's modulus of the porcine lens capsule is reported by Krag and Andreassen (1996) to be of the order of $0.15 - 0.26 \text{ N/mm}^2$; this is significantly less than the Young's modulus of 1.5 N/mm^2 for human capsules reported in Krag and Andreassen (2003). However, this difference in Young's modulus is partially offset by differences in the thickness of the capsule which (at the capsule locations corresponding to the Young's modulus data reported above) are about 60 microns for the porcine capsule (Krag and Andreassen 1996) and about 25 microns for the presbyopic human capsule (Krag et al. 1997). These considerations suggest that the porcine lens provides a useful (but not perfect) model of the human lens for the purpose of the current work.

The strains developed in the lens capsule during simulated accommodation in the ex vivo lens stretching test are strongly conditioned by the mechanical characteristics of the capsule and the way in which it interacts with the underlying lens substance. Since the testing protocol described in the current paper is limited to observations on the capsule *strains*, without any corresponding information on the local *stresses*, it is not possible to develop detailed constitutive models for the capsule (i.e. mathematical models that relate the stresses to the strains) on the basis of the current tests alone. However strain data collected using this experimental protocol – when applied to human lenses – could be used to assess the veracity of computational models of the mechanical performance of the lens in accommodation (e.g. Burd, Judge, and Cross 2002; Hermans et al. 2008). Furthermore, detailed strain measurements on the lens capsule could lead to an improved understanding of the physiological accommodative mechanism, the development and treatment of presbyopia and the improvement of interventions to treat cataracts or complications resulting from such interventions.

The proposed new experimental protocol involves the use of digital imaging correlation (DIC) techniques to measure the strains that develop in the anterior capsule during lens stretching tests. DIC techniques are well-established for the testing of engineering materials (e.g. Meunier et al. 2008) and biological tissues (e.g. the bulge tests on human skin reported by Tonge et al. 2013). A key requirement of this technique is that the surface of the material being tested must possess an appropriate texture that can be tracked as deformations occur. Surfaces without a detailed texture, such as the ocular lens, require the application of an appropriate surface layer so that the

deformations can be detected and measured. It was therefore necessary, in the initial stages of the current work, to develop suitable surface treatments for the lens.

Biological materials such as the lens capsule are typically represented in mechanical modelling procedures using a non-linear kinematic framework (Holzapfel 2000). In this framework, the deformations within the material are commonly characterized by the Green-Lagrange strain tensor. This strain measure, which is widely used to model large deformations in biological materials, represents rigid material rotations without introducing fictitious strains; it is consistent with the structural constitutive models for the lens capsule described in Burd (2009) and Burd and Regueiro (2015). Furthermore, Green-Lagrange strains conveniently revert to the conventional infinitesimal strain definitions in the limiting case of small strains. In view of these considerations, the deformations observed on the surface of the lens are interpreted using Green-Lagrange strains, referred to in the current paper as 'Green strains'.

2. Material and methods

2.1 Preliminary trials on lens surface treatments

Initial work was conducted to develop an appropriate surface preparation technique and illumination system, so that deformations occurring on the lens capsule surface during the stretching test can be captured successfully by the DIC system. In preliminary experiments, various surface treatments including the application of trypan blue, haematoxylin, eosin, methylene blue, nuclear fast red, bis-benzimidazoles, photocopier toner particles and mineral eye shimmer were tried (Fig. 1). Mineral eye shimmer with particle sizes between 10 μm and 30 μm , combined with dark field illumination, proved to be the most successful approach; this surface treatment and illumination combination was therefore employed for the main tests reported in this paper. The mineral eye shimmer used in the tests (Number 46 Twinkle, Bellapierre Cosmetics, USA) consists of mica, titanium dioxide and iron oxides. This product does not contain any vitamins, absorbents or oils that are likely to influence the water content of the lens capsule or to have other interactions.

2.2 Test procedures

Six porcine eyes (from animals that were six months old) were obtained from a local slaughterhouse in Barcelona and stored at 8°C. Eye globes were enucleated within four hours post mortem. Experiments were performed on average 24 hours post mortem (range 6 to 54 hours). Stretching tests on the lens-zonule-ciliary body were conducted using a previously-described radial

lens stretching apparatus (Michael et al. 2012; Panilla Cortés et al. 2015). Applied radial forces were measured using a sensor from a commercial digital precision balance (Precisa BJ 210C from Precisa Gravimetrics AG, Dietikon, Switzerland) allowing force readings at a resolution of 0.1 mN.

The tissue was prepared for testing in the lens stretching rig (adopting the procedures described in Michael et al. (2012) and Panilla Cortés et al. (2015)) as follows. First, eight glass beads were sutured to the sclera at 3.5 mm from the limbus with a 7-0 Prolene monofilament suture. The cornea was trephined, the iris was removed, and the sclera was cut circumferentially below the beads to isolate the anterior eye segment. Excess aqueous humor was removed from the lens surface using a micro sponge. The anterior surface was then coated with a thin layer of mineral eye shimmer particles (Fig. 1 lower right) using a 3 mm diameter round brush. A drop of balanced salt solution (BSS) was subsequently added to homogenize the particles distribution. After allowing one minute for the particles to precipitate and adhere to the anterior surface, excess particles were removed with additional BSS. The anterior segment was then placed into the experimental chamber filled with balanced salt solution. The sclera and ciliary body were radially cut to divide it into eight segments corresponding to the beads, which were then connected to the stretching hooks.

The tests were conducted in a sequence of cycles using the automatic protocol, programmed in Labview, described in Michael et al. (2012). Each test cycle consisted of 10 displacement increments of radial stretching followed by 10 displacement increments of relaxing. Each displacement increment corresponded to a radial movement of the stretching hooks of 375 microns. The time between each displacement increment and the corresponding force measurement was 10 seconds; the time between each force measurement and the application of the next displacement increment was also 10 seconds. Initially, several stretching/relaxing displacement increments were applied to establish the zero force position. Then, a preconditioning cycle was applied. This was followed by a second cycle, during which frontal images of the anterior surface of the lens were taken with a digital camera (Canon EOS 550D, 3456x2304 pixel resolution) mounted to a surgical microscope (Zeiss OPMI). During this second cycle, radial force data were recorded as described above. Frontal images were taken approximately 1 second after each radial force measurement.

For three of the six porcine lenses tested in this program, a third test cycle was then conducted; during this third cycle, Scheimpflug images of the lens cross section were captured at the end of each loading and unloading increment, using a sensor from a digital camera (Sony NEX5, 2448x1624 pixel resolution) combined with illumination and optics from a Topcon SL-45 Scheimpflug camera.

These Scheimpflug images were subsequently employed, as described later, to account for the shape of the anterior lens surface when determining the strains in the capsule. For the three tests that were conducted without the Scheimpflug images, it was not possible to conduct this shape correction.

The optical systems used to capture the frontal and Scheimpflug images were calibrated by imaging a grid placed at the same location as the lens. This calibration process provides a means of registering the Scheimpflug and frontal images for the subsequent processing of the deformation and strain data. It is noted that Scheimpflug images are subject to distortion since the object and image planes are not parallel to each other; this causes a variable magnification over the image (Huebscher et al. 1999, Dubbelman et al. 2002). These distortions were evaluated by analysing the calibration grid image. Distortions along the polar axis of the lens were found to be less than $\pm 2\%$, and distortions along the radial direction were found to be less than $\pm 4\%$. These distortion errors are regarded as being sufficiently small that they can be disregarded in the subsequent analysis.

2.3 Analysis of the frontal images

Each frontal image was processed to increase contrast and mid-tones; this image processing improved the recognition of the deformations that occurred on the lens surface. Images of the speckle pattern on the lens surface, obtained at different stages in the test were processed using GOM Aramis, (GOM GmbH, Braunschweig, Germany) which is a bespoke commercial DIC software system. Images of the speckle pattern were compared to the initial (unstretched) configuration (e.g. Tyson et al. 2002) to determine the spatial variation of displacements in the anterior capsule as the lens is stretched; the Green strains were determined from this displacement field, automatically, by the GOM Aramis software. It should be noted that the displacements and strains determined in this way – which are referred to in this paper as ‘projected displacements’ and ‘projected strains’ respectively - relate to a projection onto a frontal plane rather than relating to displacements and strains actually occurring in the plane of the capsule.

Fig. 2a shows the field of projected strains presented in terms of an equivalent strain measure known as ‘Mises strain’ (which is a strain metric that quantifies the local distortion induced in the material) obtained for one of the porcine lenses in the test program when subjected to a relatively large radial stretch. This projected Mises strain field provides confirmation that the deformations induced in the capsule are approximately axially symmetric (as indicated by the approximately circular nature of the strain contours in Fig. 2a). However, small departures from axial symmetry in

the geometry of the lens, zonules, or the load application system employed in the tests, may mean that the precise location of the axis of symmetry of the projected Mises strain field (indicated as Co in Fig. 2) will differ slightly from the geometrical polar axis of the lens. The strains measured at points near the equator may not actually relate to the lens capsule. The projected Mises strains in Fig. 2a appear to increase rapidly with radial position near to the lens equator. This is because, in the vicinity of the lens equator, most of the eye shimmer particles rest on the zonules and not on the underlying lens capsule. The inferred strains in the equatorial region therefore relate to those that are developed in the (relatively flexible) zonules, rather than in the underlying lens.

To further process the data, the location of the axis of symmetry, Co , needs to be determined at each increment in the test. To estimate the coordinates (x_{co}, y_{co}) of Co in terms of a coordinate system (x, y) fixed in the frontal plane (Fig 2b), the field of projected Mises strains, ϵ^{Mises} , is approximated by the spherical paraboloid $\epsilon^{approx}(x, y)$:

$$\epsilon^{approx}(x, y) = \frac{(y-y_{co})^2 + (x-x_{co})^2}{k_1} + k_2 \quad (1)$$

where k_1 and k_2 are parameters to be determined. Values of the coordinates (x_{co}, y_{co}) and the parameters k_1 and k_2 are determined by finding a best fit to the observed Mises strain data; coefficients of determination of 0.92 or above were considered acceptable.

The coordinates of Co when determined in this way were typically found to vary slightly during the test. This is presumed to be partly due to small translations of the lens during the test and partly due to errors in the fit between the measured strain data and the spherical paraboloid approximation. To minimize these effects, a procedure was developed in which the location (x_{co}, y_{co}) of Co at maximal stretch is initially found (using the fitting process described above). This location is then registered with respect to the square grid of DIC grid points that is automatically computed on the surface speckle pattern, in the frontal plane, by the GOM Aramis software. Specifically, the position of Co with respect to the four DIC grid points immediately surrounding it is established by the geometric approach illustrated in Fig. 3. Once this relative position has been established, the absolute location of Co at all other stages on the test is determined by interpolation from the DIC grid.

2.4 Scheimpflug image processing

Data from the Scheimpflug images were used to determine the anterior shape of the lens at each increment in the loading cycle. These shape data facilitate the conversion of the projected strains determined from the frontal images into strains acting in the plane of the capsule. To determine the required data on lens shape and to register the frontal and Scheimpflug images, the following procedures were adopted.

The Scheimpflug images were converted to greyscale and then transformed into binary images. Hence all greys darker than a certain threshold were converted into black and, conversely, all greys lighter than a certain threshold were converted into white. In the Scheimpflug images, the anterior lens capsule surface appeared considerably brighter than the rest of the lens, due to the presence of mineral eye shimmer particles. This facilitated an accurate and clear detection of the lens capsule outline when selecting an appropriate threshold for the conversion to a binary image. The lens capsule surface was identified as the transition from black to white in the binary images.

The frontal and Scheimpflug images were registered with each other by assuming that the lens deforms in an axially symmetric manner during the stretching process, with an axis of symmetry at C_0 for the frontal images and at the lens anterior pole for the Scheimpflug images. To process the Scheimpflug images, a cylindrical coordinate system, (r, z) was adopted as shown in Fig. 4.

The shape of one-half of the lens capsule surface, as observed in the Scheimpflug images, at each displacement increment in the test was represented by the quartic function,

$$z(r) = ar^4 + br^3 + cr^2 + dr + e \quad (2)$$

where the constants a, b, c, d, e were determined by least squares fit with the Scheimpflug image. Curve fittings with coefficients of determination of 0.99 or above were considered acceptable. The use of quartic functions to represent the lens anterior outline allowed for an accurate fitting in both the central and peripheral areas of the lens. It is noted that, since the function in Equation (2) includes odd components, it can only be used to provide a fit to one-half of the lens profile. A polynomial function to represent the lens cross section outline in lens stretching tests was also used by Pierscionek (1995), although in this case a quadratic was employed. For the current work, quadratic functions were found to be unsatisfactory for the strain analysis process, particularly in the peripheral regions of the lens. The quartic function in Equation (2), however, was found to perform satisfactorily in this application.

2.5 Strain analysis

At each displacement increment, the field of projected Green strains in a Cartesian basis were computed automatically by GOM Aramis. These strain data were further processed in polar coordinates with origin at Co as follows. The coordinates (projected onto the frontal plane) (x,y) of each data point and the corresponding components of the projected Green strain tensor E_{ij} , $i,j = x,y$ at each stretching increment were then computed. The strains were then transformed into a polar coordinate basis (Fig. 2b) via the equations:

$$r = \sqrt{(x - x_{co})^2 + (y - y_{co})^2} \quad (3)$$

$$\theta = \tan^{-1} \left(\frac{y - y_{co}}{x - x_{co}} \right) \quad (4)$$

$$\begin{bmatrix} E_{r\theta} & 0 \\ E_{\theta\theta} & 0 \\ 0 & 1 \end{bmatrix} = \begin{bmatrix} \cos \theta & \sin \theta & 0 \\ -\sin \theta & \cos \theta & 0 \\ 0 & 0 & 1 \end{bmatrix} \begin{bmatrix} E_{xx} & E_{xy} & 0 \\ E_{yx} & E_{yy} & 0 \\ 0 & 0 & 1 \end{bmatrix} \begin{bmatrix} \cos \theta & -\sin \theta & 0 \\ \sin \theta & \cos \theta & 0 \\ 0 & 0 & 1 \end{bmatrix} \quad (5)$$

where E_{ij} , $i,j = x,y$ are the projected Green strains in Cartesian coordinates and E_{ij} , $i,j = r,\theta$ are the projected Green strains in polar coordinates.

The radial strains E_{rr} obtained from this process relate to a projection onto the frontal plane. Since the curvature of the lens surface changes during the test, these projected strains cannot be used, directly, to infer the strains actually developed in the local plane of the capsule. A correction was therefore applied to this strain component. As a consequence of the axial symmetry in the strain field, however, the circumferential strains $E_{\theta\theta}$ in the plane of the capsule are identically equal to the projected circumferential strains and so a correction does not need to be applied to this strain component.

To determine the Green strains in the plane of the capsule (rather than the projected Green strains) consideration needs to be given to the cross section shape of the lens at each increment of the test. Fig. 4 indicates a representation of the kinematics of an arbitrary material point P on the anterior capsule surface. In the unstretched state (Fig. 4a), the coordinates of P are (R, Z) ; in the stretched state (Fig. 4b) the coordinates of P are (r,z) . The location of P in the unstretched state may also be represented by the meridional curvilinear coordinate S, which relates to distance along the lens meridian from the anterior pole. In the stretched state, the meridional coordinate of P is s.

To proceed, it is assumed that the strain field is axially symmetric and so the shear strains $E_{r\theta}$ and $E_{\theta r}$ (determined from Eqn. (5)) are assumed to be small and are therefore neglected. The circumferential strains in the plane of the capsule are equal to the projected circumferential strains $E_{\theta\theta}$ determined using Eqn. (5). To determine the meridional strain in the plane of the capsule, E_{ss} , however, analysis is needed, as described below, based on the shape of the anterior capsule.

The meridional stretch ratio, λ_m , and the radial stretch ratio λ_r , are defined,

$$\lambda_m = \frac{ds}{dS}; \quad \lambda_r = \frac{dr}{dR} \quad (6)$$

These stretch ratios are related by,

$$\lambda_m = \eta \lambda_r; \quad \eta = \frac{\cos A}{\cos a} \quad (7)$$

where $\cos A = \frac{dR}{ds}$ and $\cos a = \frac{dr}{ds}$ may be determined directly from the local slope of the capsule as determined from the Scheimpflug images. The meridional Green strain, E_{ss} , and the radial projected Green strain, E_{rr} (determined from Eqn. (5)) on the basis of standard definitions are,

$$E_{ss} = \frac{1}{2} ([\lambda_m]^2 - 1); \quad E_{rr} = \frac{1}{2} ([\lambda_r]^2 - 1) \quad (8)$$

The meridional Green strain is therefore determined from the projected value of E_{rr} using,

$$E_{ss} = \frac{1}{2} (2\eta^2 E_{rr} + \eta^2 - 1) \quad (9)$$

Values of $\eta(R)$ for use in Equation (9) at each displacement increment in the test were determined from,

$$\eta(R) = \frac{\cos A(R)}{\cos a(r)} \quad (10)$$

where the mapping $r(R)$ was determined using the field of radial displacements determined from the observed projected deformations in the frontal plane and $\cos A$, $\cos a$ were determined from the quartic polynomials used to represent the shape of the anterior surface.

It was found that near the lens pole the correction factor η was invariably close to unity, indicating that the need for strain correction in these regions is minimal. The correction factor is more significant, however, for points on the lens near to the equator.

3. Results and discussion

3.1 Normalized initial radius

Data are presented below on the measured strains at three representative radial distances from the lens pole. These radial distances are specified in terms of normalized initial radius, R/R_L , where R is the radial coordinate of a material point on the lens in the initial (undeformed) configuration and R_L as the radius of the undeformed lens. Three representative values of normalized initial radius, $R/R_L = 0.4, 0.6$ and 0.8 , (Fig. 2b) have been selected for data presentation purposes.

3.2 Scheimpflug images

Best-fit quartic outlines for the three lenses for which Scheimpflug images were captured are shown in Fig. 5. Data are also indicated on the values of radial force corresponding to each outline. In all cases, as the lens is stretched, the shape flattens in peripheral regions with minimal shape changes occurring near to the lens pole.

It should be noted that the anterior lens surface outlines shown in Fig. 5 exclude the equatorial region of the lens. This is because the eye shimmer particles applied to peripheral regions of the lens tended to rest on the zonules rather than the underlying lens surface; as a consequence, the lens surface in the region between the zonular attachments and the equator could not be reliably identified from the Scheimpflug images. For this reason, Fig. 5 does not indicate the profile for the entire anterior lens surface.

3.3 Green strains on the anterior lens surface

Projected Green strains in a polar coordinates basis for all of the lens stretching tests were determined using the procedures outlined in Section 2. Consistent with the axially symmetric nature of the tests, the shear strains ($E_{r\theta}$ and $E_{\theta r}$) were found to be negligible (typically less than 10^{-3}). Also, the circumferential and radial projected strains were invariably found to conform closely to axial symmetry about the polar axis.

For the three lenses for which Scheimpflug images were obtained, further processing was used to determine the meridional strains E_{ss} . It was found that for $R/R_L = 0.4$ and 0.6 the correction

factor η was close to unity, indicating that the need for strain correction in these regions is minimal. For $R/R_L = 0.8$ the correction factor was typically found to be in the region of 0.95 for a maximally stretched lens.

The circumferential strains $E_{\theta\theta}$ and the meridional strains E_{ss} for an example lens, Sample #18, at maximal stretching are shown in Fig. 6 for the three representative values of normalized initial radius. Consistent with data obtained from the other lenses, the data show a broadly axially symmetric pattern of circumferential and meridional strains with respect to the lens polar axis. The magnitude of both strain components increases with distance from the polar axis.

Some of the data in the peripheral regions of the lens (i.e. for $R/R_L = 0.8$) are seen to be missing in Fig. 6. This is due to difficulties in achieving a uniform coverage of mineral eye shimmer particles near the equatorial region of the lens where the slope of the lens surface is relatively large. It is noted that achieving a surface texture that provided an adequate coverage over the entire lens proved to be a significant difficulty and that considerable experimentation (in the initial stages of the project) was needed to achieve a surface treatment that was able to provide complete (or almost complete) data on the capsule strains.

3.4 Mechanical response of the porcine lenses

Relationships between the applied radial force and the associated circumferential and meridional Green strains at the three representative values of normalized radius are shown Fig. 7. The strain data indicated in this figure were determined by computing mean strain values along circular loci corresponding to each normalized initial radius. Meridional strains were obtained only for the three experiments for which Scheimpflug images were recorded while circumferential strains were evaluated for all of the samples.

The data indicate that the combined capsule/lens tends to stiffen during the stretching process (i.e. the slope of the force – strain curve increases with increasing strain). The results also indicate hysteretic behaviour (i.e. unloading occurs along a path that differs from the loading path). Hysteresis appears to be more significant for the circumferential than the meridional strains. These features of the response are associated with the combined action of the capsule and the underlying lens substance, although it is presumed that the influence of the lens substance is relatively minor. The non-linear response in Fig. 7 is typical of biological materials and is consistent with the stiffening response of the capsule observed in previous tests on porcine lenses described in Krag and

Andreassen (1996). It is also noted that the hysteresis behaviour shown in Fig 7 is consistent with the data for human capsules given in Krag and Andreassen (2003). It may prove necessary to consider the effects of hysteresis in future developments of constitutive models for the capsule and/or the lens substance.

The data in Fig. 7 show considerable variability, especially for the circumferential strains at large values of imposed radial stretch. Also, the response of Sample #23 appears anomalous. The anomalies in the Sample #23 data are thought to be caused by a departure from axial symmetry in the applied radial loading. This departure from symmetry induced slight movements of the lens (approximately 0.35 mm and 0.38 mm during the loading and unloading phases of the test cycle respectively). These movements seem to have affected the circumferential strains more significantly than the meridional strains.

The source of variability apparent in Fig. 7 for the other tests is unclear. Differences in post mortem time are unlikely to provide an explanation, since Samples #18 and #24 were tested with relatively dissimilar post mortem times, (6 hours and 54 hours respectively) and yet the force-strain response of these two samples is similar. (The other samples were all tested at approximately 24 hours post mortem.) All the lenses were harvested from six-month old animals from the same breed, they had similar diameters (between 9.2 and 10.1 mm) and normal morphology. There were therefore no obvious differences between the lenses that were tested. It is concluded, therefore, that the variability in the force-strain data is most likely due to natural differences in the samples, combined with minor differences in the setting up of each specimen prior to the experiments.

3.5 Radial distribution of lens capsule strains

Fig. 8 indicates the circumferential and meridional strains, at the three representative values of normalized initial radius, corresponding to a reference radial stretching force of 100 mN. The strain data corresponding to this value of reference force were determined by linear interpolation of the data in Fig 7.

Fig 8. indicates a clear tendency for the meridional strains to be greater in magnitude than those in the circumferential direction. It is emphasised, however, that this does not constitute evidence of material anisotropy in the capsule, since the mechanical response of the capsule in the lens stretching test is partly determined by the local surface curvatures (which are anisotropic as a

consequence of the non-spherical shape of the lens) and partly by the detailed constitutive behaviour of the capsule.

It is also evident from Fig. 8 that the strains increase with increasing distance from the lens pole; this is especially the case for the meridional strains. It is noted that it is not possible, from these data alone, to make any inferences on the likely spatial variation in capsule and/or lens substance material properties.

4. Conclusions

A previously-published lens stretching protocol has been further developed to include procedures to measure the strains developed in the lens capsule when radial stretching forces are applied. Initial experimentation was required to develop a surface treatment and illumination system that provided a texture that is sufficiently detailed and uniform to enable the surface deformations to be tracked with a DIC system based on frontal images of the lens. Once a suitable protocol had been developed, it was used to conduct tests on six porcine lenses. For three of the lenses, additional Scheimpflug images were taken of the lens cross section to allow the in-plane meridional strains to be computed. The inferred spatial distribution of strains provides significantly more insight into the kinematic performance of the lens than more conventional forms of the lens stretching test.

The main outcome of the study is a demonstration of the viability of conducting lens stretching experiments with simultaneous direct measurements of the strains developed in the capsule. The resulting protocols are suitable for application to human lenses for future biomechanical studies on the mechanics of the lens. It is noted that surface measurements of capsule strains under conditions of ex vivo simulated accommodation cannot, solely, form a basis for new constitutive models of capsule behaviour. This is on the basis that information is not available on the stresses acting in the capsule and that the observed strains are influenced by the interaction between the capsule and the lens substance. Kinematic data obtained from this proposed testing protocol could, however, be compared with computational models of the lens to check their veracity.

Improved forms of the experiment involving stereo cameras are also possible; this will also form the basis of future work.

Certain broad conclusions can be drawn on the behaviour of the porcine lenses tested in this program as follows. Consistent with most biological tissues, the capsule strains were found to

increase a non-linear way with increasing radial force. The capsule strains indicated hysteretic behaviour (in which the loading and unloading paths are different). It may prove necessary to allow for hysteretic behaviour when developing future constitutive models for the capsule and/or the lens substance.

Acknowledgements

We are grateful to Gustavo A. Montenegro for help and valuable comments during the preparation of the present study. This research did not receive any specific grant from funding agencies in the public, commercial, or not-for-profit sectors.

Figure Captions

Fig. 1; Frontal images of porcine lenses with trial surface treatments: trypan blue (top left), haematoxylin (top centre), methylene blue (top right), toner particles (bottom left) and mineral eye shimmer (bottom centre and right).

Fig. 2; (a) Contour plot of a representative projected Mises strain field (for Sample #15). (b) schematic representation of the lens perimeter, the location of the axis of symmetry for the strain field (Co) and the frontal plane Cartesian (x,y) and polar (r,θ) coordinate systems. The dotted circles represent the locus of points at representative values of normalized initial radius R/R_L equal to 0.4, 0.6 and 0.8 respectively (where R is the initial radial position of a material point in the unstretched configuration and R_L is the equatorial radius of the unstretched lens).

Fig. 3; Determination of the location of the axis of symmetry for the strain field Co in relation to the four digital image correlation (DIC) grid points surrounding it (a,b,c,d intersections of interpolation lines with the DIC facet surrounding Co ; a/b and c/d are assumed constant during stretching)

Fig. 4; Kinematic representation of the deformation of the anterior lens surface during stretching; (a) shows the lens in the initial (unstretched) state; (b) shows the lens in the stretched state. Symbols are defined in the text.

Fig. 5; Anterior lens surface outlines determined from the Scheimpflug images at different values of radial force during stretching: a) Sample #18, b) Sample #23, c) Sample #24. Note that the outlines do not include the equatorial region of the lens.

Fig. 6; (a) Circumferential strains $E_{\theta\theta}$ and (b) meridional strains E_{ss} measured at maximal stretching, Sample #18, along three circular loci at normalized initial radius R/R_L equal to 0.4 (orange), 0.6 (cyan) and 0.8 (green).

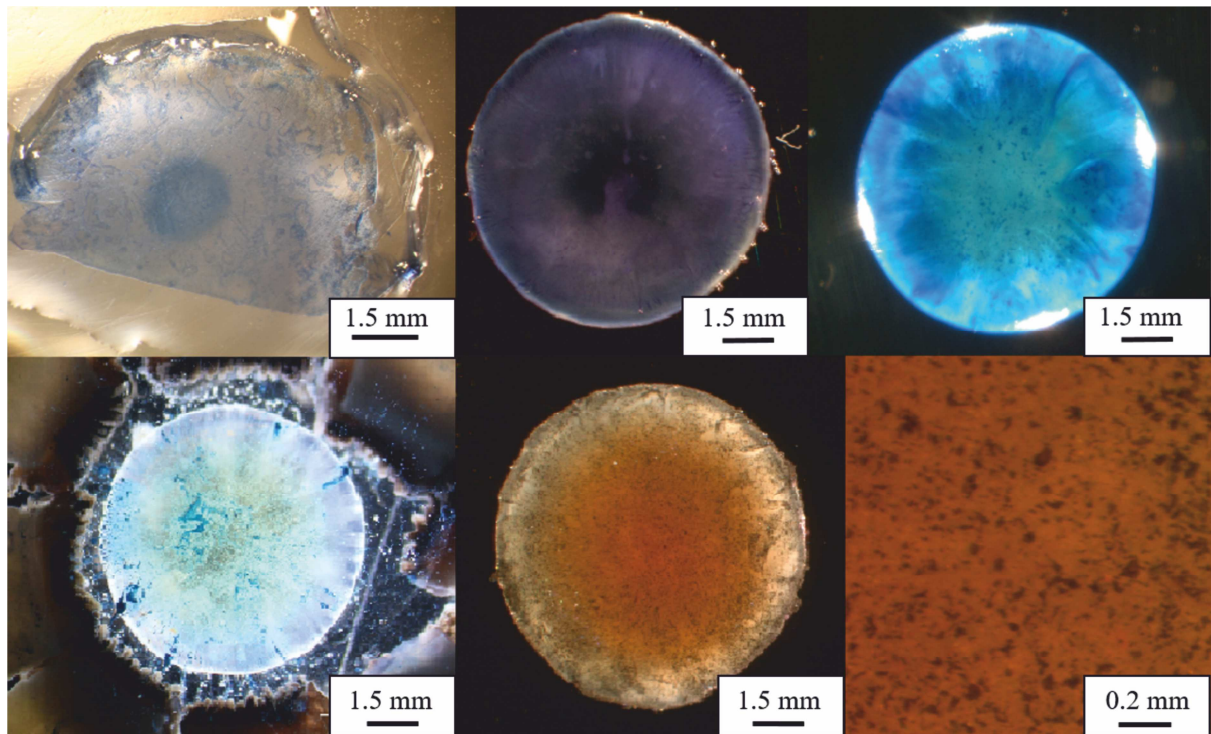
Fig. 7; Force versus circumferential strain $E_{\theta\theta}$ (a,c,e) and meridional strain E_{ss} (b,d,f) determined for the lens samples during stretching. Strains were computed along three circular loci initially located at normalized initial radius R/R_L equal to 0.4 (a,b), 0.6 (c,d) and 0.8 (e,f).

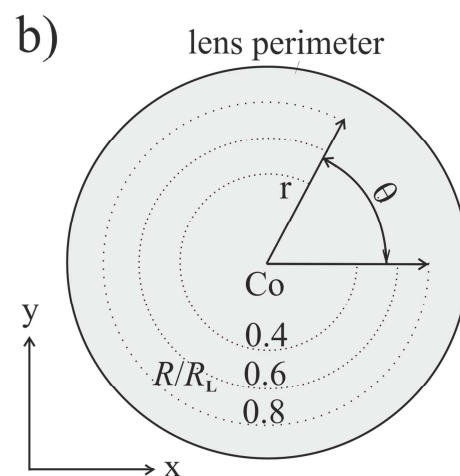
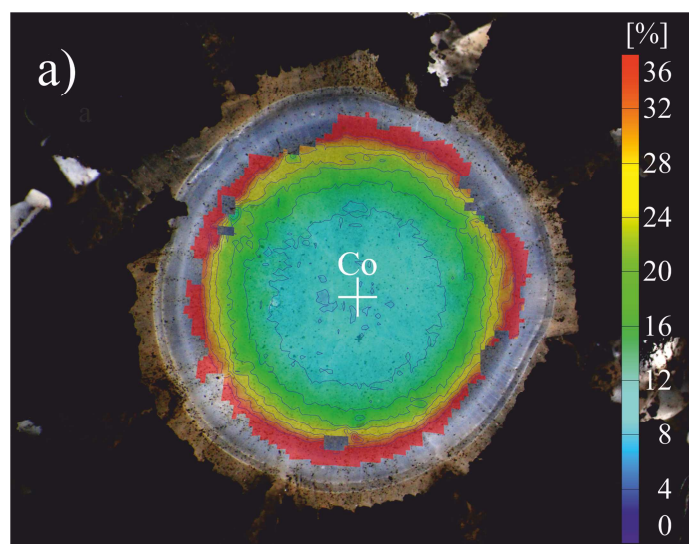
Fig. 8; Interpolated data on circumferential strain $E_{\theta\theta}$ and meridional strain E_{ss} for all tests for an applied radial load of 100 mN. Data from individual tests are shown as symbols. Averaged data are shown as columns.

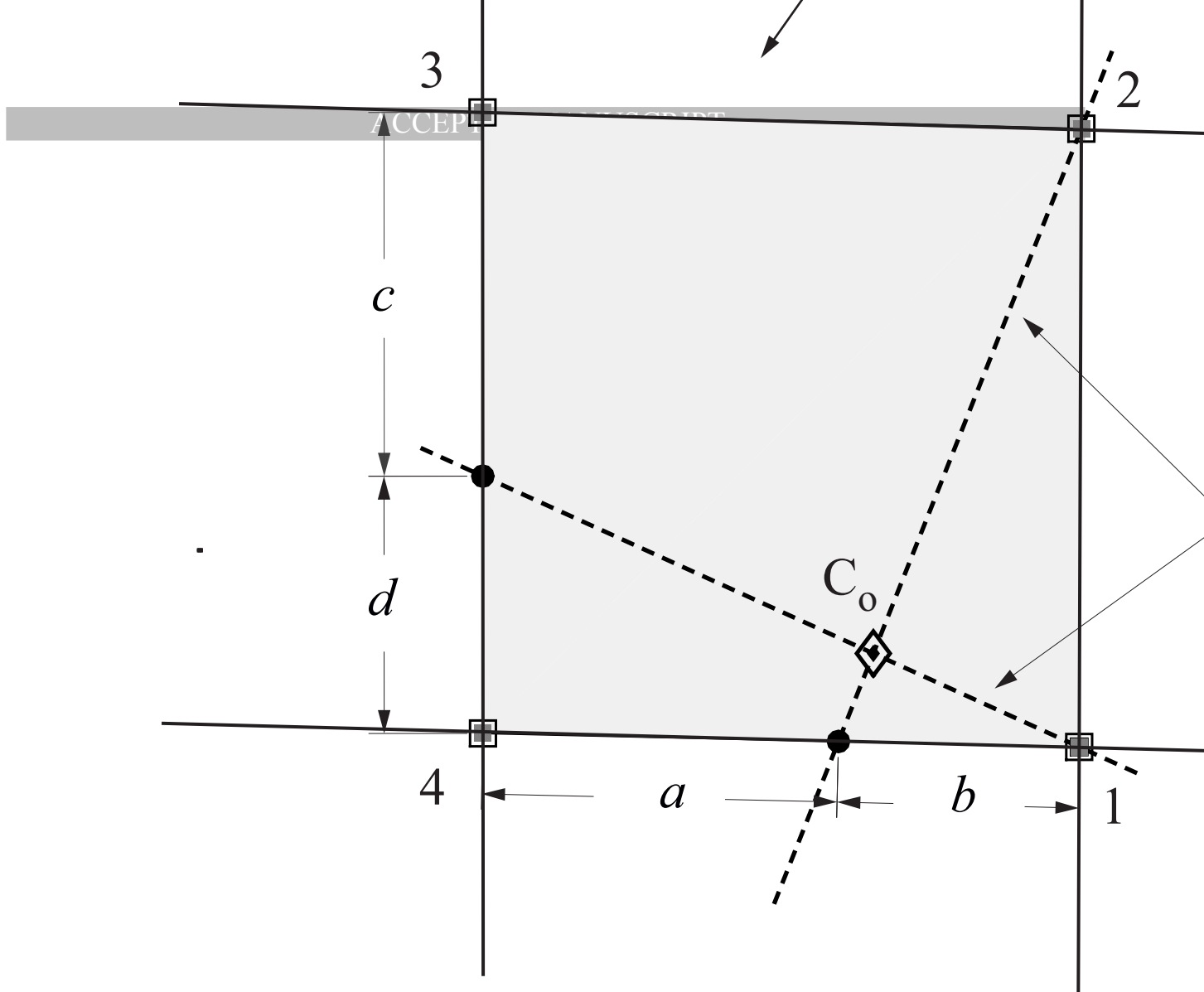
References

- Augusteyn, R.C., Mohamed, A., Nankivil D., Veerendranath P., Arrieta E., Taneja M., Manns F., Ho A., Parel. J.-M., 2011. Age-dependence of the optomechanical responses of ex vivo human lenses from India and the USA, and the force required to produce these in a lens stretcher: The similarity to in vivo disaccommodation, *Vision Research* 51, 1667-78.
- Burd, H.J., 2009. A structural constitutive model for the human lens capsule. *Biomechanics Model. Mechanobiol.* 8, 217-231.
- Burd, H.J., Judge, S.J., Cross, J.A., 2002. Numerical modelling of the accommodating lens. *Vision Research* 42(18), 2235-2251.
- Burd, H.J., Regueiro, R.A., 2015. Finite element implementation of a multiscale model of the human lens capsule. *Biomechanics Model. Mechanobiol.* 1-16.
- Dubbelman, M., Weeber, H. A., van der Heijde, G.L., & Völker-Dieben, H. J. 2002. Radius and asphericity of the posterior corneal surface determined by corrected Scheimpflug photography. *Acta Ophthalmologica Scandinavica*, 80(4), 379-383.
- Hahn, J., Fromm, M., Halabi, F. A., Besdo, S., Lubatschowski, H., Ripken, T., & Krüger, A. (2015). Measurement of Ex Vivo Porcine Lens Shape During Simulated Accommodation, Before and After fs-Laser Treatment. *Lens Shape During Accommodation Post fs-Laser. Investigative ophthalmology & visual science*, 56(9), 5332-5343.
- Hermans, E.A., Dubbelman, M., van der Heijde, G.L., Heethaar, R.M., 2008. Change in the accommodative force on the lens of the human eye with age. *Vision Research* 48, 119-126.
- Heys, K.R., Cram, S.L., Truscott, R.J.W., 2004. Massive increase in the stiffness of the human lens nucleus with age: the basis for presbyopia? *Molecular Vision* 10, 956-963.
- Holzapfel, G.A. 2000. *Nonlinear solid mechanics: a continuum approach for engineering* (John Wiley: Chichester).
- Huebscher, H. J., Fink, W., Steinbrück, D., & Seiler, T. 1999. Scheimpflug records without distortion—a mythos?. *Ophthalmic Research*, 31(2), 134-139.
- Krag, S., Andreassen, T.T., 1996. Biomechanical measurements of the porcine lens capsule. *Exp. Eye Res.* 62, 253-260.
- Krag, S., Olsen, T., Andreassen, T.T., 1997. Biomechanical characteristics of the human anterior lens capsule in relation to age. *Investigative Ophthalmology and Visual Science* 38, 357-363.
- Krag, S., Andreassen, T.T., 2003. Mechanical properties of the human lens capsule. *Progress in Retinal and Eye Research* 22, 749-767.
- Manns, F., J. M. Parel, D. Denham, C. Billotte, N. Ziebarth, D. Borja, V. Fernandez, M. Aly, E. Arrieta, A. Ho, and B. Holden. 2007. 'Optomechanical response of human and monkey lenses in a lens stretcher', *Invest. Ophthalmol. Vis. Sci.*, 48: 3260-68.
- Meunier, L, G Chagnon, D Favier, L Orgéas, and P Vacher. 2008. 'Mechanical experimental characterisation and numerical modelling of an unfilled silicone rubber', *Polymer Testing*, 27: 765-77.
- Michael, R., Mikieliewicz, M., Gordillo, C., Montenegro, G.A., Pinilla Cortes, L., Barraquer, R.I., 2012. Elastic Properties of Human Lens Zonules as a Function of Age in Presbyopes. *Invest. Ophthalmol. Vis. Sci.* 53, 6109-6114.
- Moffat, B.A., Atchison, D.A., Pope, J.M., 2002. Age-related changes in refractive index distribution and power of the human lens as measured by magnetic resonance micro-imaging in vitro. *Vision Research* 42, 1683-1693.
- Panilla Cortés, L., Burd, H.J., Montenegro, G.A., D'Antin, J.C., Mikieliewicz, M., Barraquer, R.I., Michael, R., 2015. Experimental Protocols for Ex Vivo Lens Stretching Tests to Investigate the

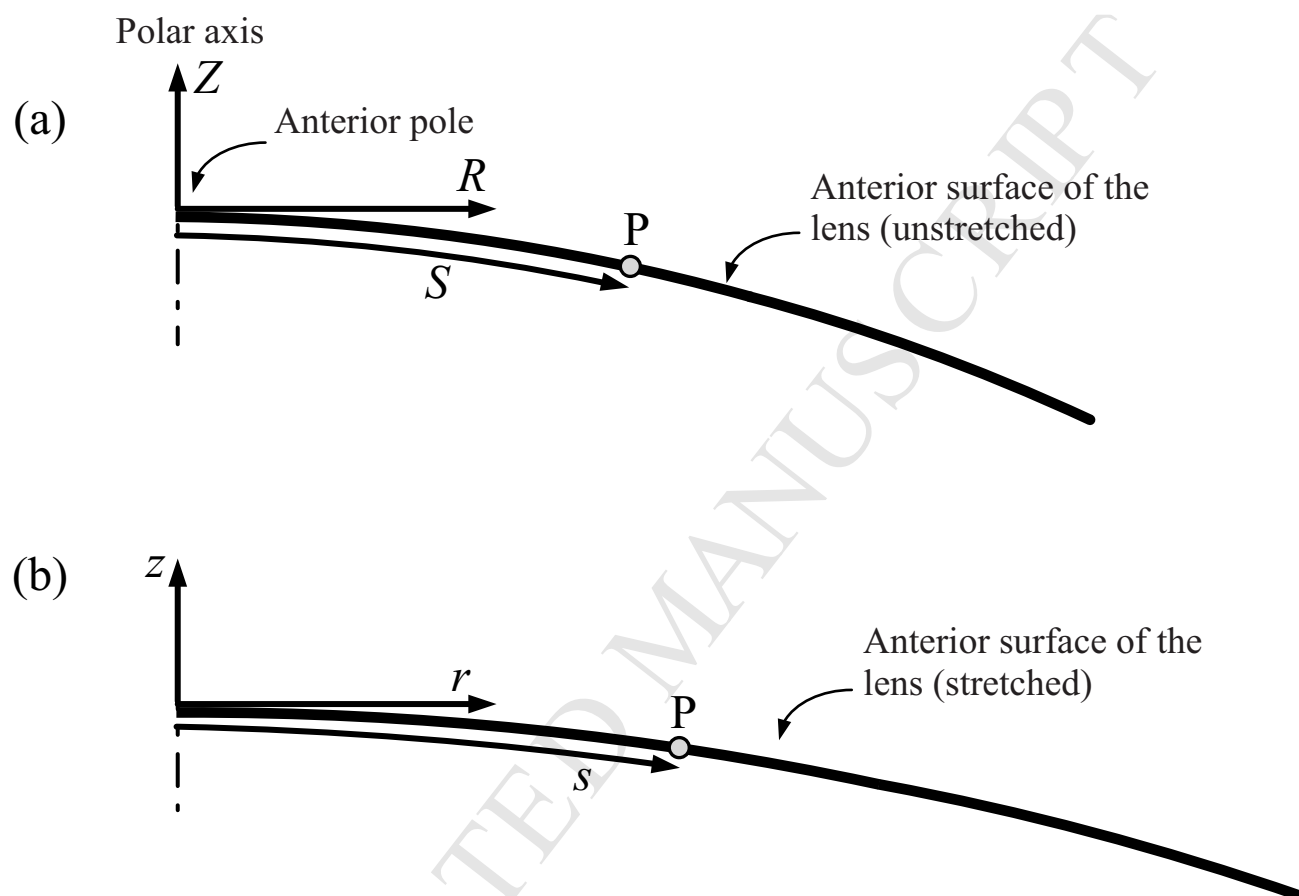
- Biomechanics of the Human Accommodation Apparatus: Alternative Protocols for Lens Stretching Tests. *Invest. Ophthalmol. Vis. Sci.* 56, 2926-2932.
- Pierscionek, B.K., 1995. Age-related response of human lenses to stretching forces. *Exp. Eye Res.* 60, 325-332.
- Pierscionek, B., Belaidi, A., Bruun, H., 2005. Refractive index distribution in the porcine eye lens for 532 nm and 633 nm light. *Eye* 19, 375-381.
- Reilly, M. A., Hamilton, P. D., Perry, G., & Ravi, N. (2009). Comparison of the behavior of natural and refilled porcine lenses in a robotic lens stretcher. *Experimental eye research*, 88(3), 483-494.
- Reilly, M., Ravi, N., 2009. Microindentation of the young porcine ocular lens. *J. Biomechanical Engineering* 131.
- Sanchez, I., Martin, R., Ussa, F., Fernandez-Bueno, I., 2011. The parameters of the porcine eyeball. *Graefe's Archive for Clinical and Experimental Ophthalmology* 249, 475-482.
- Sueiras, V. M., Moy, V. T., & Ziebarth, N. M. (2015). Lens capsule structure assessed with atomic force microscopy. *Molecular vision*, 21, 316.
- Tonge, Theresa K, Lorre S Atlan, Liming M Voo, and Thao D Nguyen. 2013. 'Full-field bulge test for planar anisotropic tissues: Part I-Experimental methods applied to human skin tissue', *Acta Biomaterialia*, 9: 5913-25.
- Tyson, J., Schmidt, T., & Galanulis, K. 2002. Biomechanics deformation and strain measurements with 3D image correlation photogrammetry. *Experimental Techniques*, 26(5), 39-42.
- Weeber, H.A., vanr Heijde, G.L., 2007. On the relationship between lens stiffness and accommodative amplitude. *Exp. Eye Res.* 85, 602-607.
- Ziebarth, N.M., Borja, D., Arrieta, E., Aly, M., Manns, F., Dortonne, I., Nankivil, D., Jain, R., Parel, J.M., 2008. Role of the lens capsule on the mechanical accommodative response in a lens stretcher. *Invest. Ophthalmol. Vis. Sci.* 49, 4490-4496.



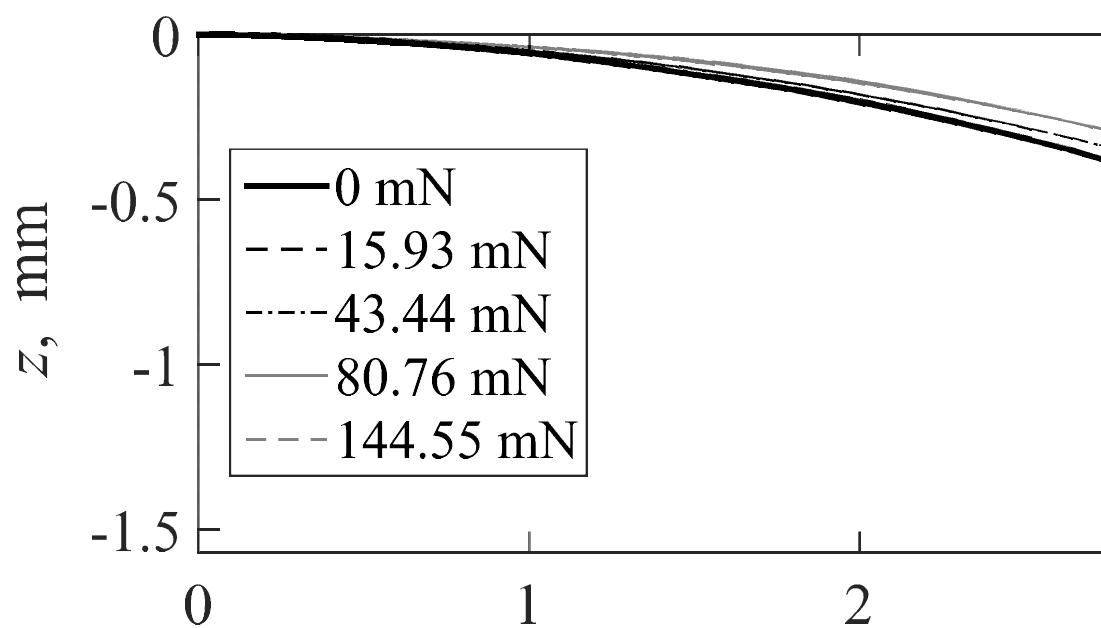




□ = DIC grid points

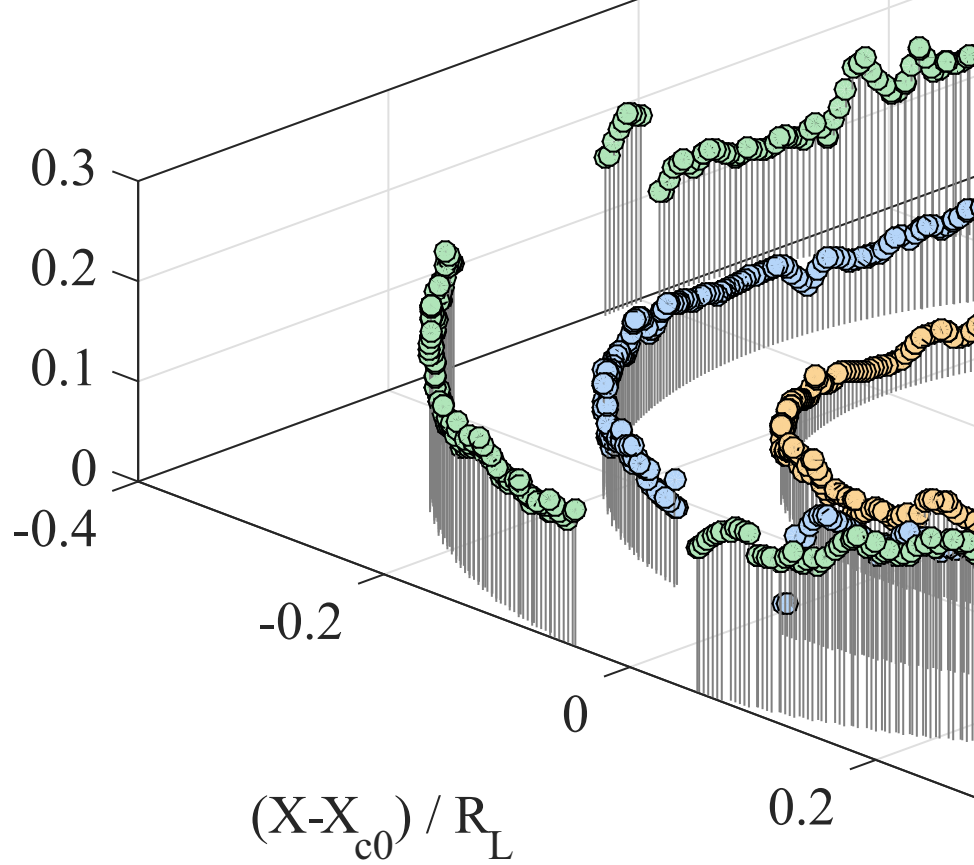


c)





meridional strain, Green



ACCEPTED MANUSCRIPT

